Progress in Nuclear Energy 154 (2022) 104469

Contents lists available at ScienceDirect

Progress in Nuclear Energy

journal homepage: www.elsevier.com/locate/pnucene

A non-destructive model for thermal-hydraulics of wire-wrapped rod bundle and wire-rod contact corner microscopic behavior

Junren Hou, Qingkang Song, Haojie Leng, Chaohui Xue, Yuan Yuan, Yuan Zhou *

College of Physics, Sichuan University, Chengdu, 610065, China

ARTICLE INFO

Keywords:
Supercritical water
High-fidelity model
Thermal-hydraulic characteristics
Microscopic behavior

ABSTRACT

Wire-wrapped rod bundle numerical simulation relates to multiscale parameters, such as axial length of the rod bundle (600 mm) and wire-rod contact corner (0.4 mm). The existing studies tend to adopt the embedding approximation wire model, which cannot simulate microscopic behavior at the wire-rod contact corner and bring the uncertainty of numerical models. To simulate the actual situation of the wire-wrapped rod bundle, this paper established a high-precision non-destructive wrapped wire model based on virtual ellipse flow surfaces and fillet connection and then investigated the thermal-hydraulics of the wire-wrapped rod bundle and microscopic behavior at wire-rod contact corner at the working pressure of 25 MPa, inlet temperature of 692.45 K, mass flux of 1000 kg/m^2·s, and heat flux of 400 kW/m^2. The influence of the distance of wire embedded into the rod bundle on heat transfer and pressure drop was quantitatively analyzed. ω-RSM turbulence model is used due to its higher prediction accuracy in the high enthalpy region (enthalpy >2700 kJ/kg). The result shows that numerical simulation has a good agreement with the experimental data. Compared with embedding approximation models, the high-fidelity non-destructive wrapped wire model shows better heat transfer and greater friction resistance. The wire-wrapped rod bundle increased the heat transfer coefficient by 14% and increased the friction factor by 10% compared with the bare rod bundle. A dead-water area exists at the wire-rod contact corner with the phenomena of low velocity, poor heat transfer and high fluid temperature. This numerical investigation helps to optimize the wire structure design while providing insight into the influence of wire.

1. Introduction

The fourth-generation nuclear reactor system (Gen IV) is a theoretical nuclear reactor proposed at the annual meeting of the American Nuclear Society in June 1999 (DoE, 2002). The supercritical water reactor (Squarer et al., 2003) is a high-temperature and high-pressure water reactor whose working environment is operating above the thermodynamic critical point of water (647 K, 22.1 MPa). Supercritical water has both gaseous and liquid properties, and its thermal conductivity is significantly higher than other light waters. The characteristics of supercritical water make supercritical water reactor have the advantages of high thermal efficiency and low cost. These advantages of supercritical water reactors show broad development prospects.

Since 1990 there were lots of investigations on the core model of supercritical water reactors. A. Yamaji et al. (Yamaji, 2001) and Y. Oka et al. (Oka et al., 2002) proposed a square core arrangement and found the square fuel assembly structure makes the power distribution more uniform. In 2003, X. Cheng et al. (Cheng et al., 2003) found square structure has a tighter lattice through sub-channel analysis. In 2007, J. Hofmeister et al. (Hofmeister et al., 2007) measured the heat transfer characteristics of high-performance light water reactors to verify the advantages of square reactors for more uniform power distribution. M. Zhao et al. (Zhao et al., 2012) and H. Wang et al. (Wang et al., 2014) experimentally investigated the heat transfer of the 2 × 2 bare rod bundle inside a square channel. The result shows that the circumferential wall temperature distribution is uneven, the highest wall temperature appears in the corner sub-channel, and the lowest wall temperature appears in the interior sub-channel. Gu et al. (Gu et al., 2015) also experimentally studied the heat transfer characteristics of supercritical water in a 2 × 2 bare rod bundle. It is found that the effects of heat flux, mass flux and pressure on the internal heat transfer behavior of the 2 × 2 rod bundle are similar to those observed in the tubes. In 2016, H. Wang et al. (Wang et al., 2016) and H.-Y. Gu et al. (Gu et al., 2016) both conducted experimental studies on heat transfer to supercritical water flowing in a 2 × 2 rod bundle inside a square channel with rounded corners. Gu et al. found that the swirling flow around the wire enhances heat transfer. Wang et al. found that wrapped wire reduces the

* Corresponding author.
E-mail address: zhouyuan1911@126.com (Y. Zhou).

https://doi.org/10.1016/j.pnucene.2022.104469
Received 9 June 2022; Received in revised form 8 September 2022; Accepted 11 October 2022
0149-1970/© 2022 Elsevier Ltd. All rights reserved.

Nomenclature

A	area, m^2
c_p	specific heat, J/kg·K
d	distance of the wire embedding into the rod bundle, mm
f	friction factor
G	mass flux, kg/m^2·s
h	heat transfer coefficient, W/(m^2·K)
k	thermal conductivity, W/m·K
p	pressure, Pa
P	heat power, kW
q	heat flux, kW/m^2
q_v	heat generation rate, kW/m^3
S	surface area, m^2
T	temperature, K
$\overline{T}$	mean temperature, K
V	volume, m^3
v	velocity, m/s
v_{cross}	cross-sectional velocity, m/s
W	mass flow rate, kg/s
z	axial distance, mm

Greek letters

ρ	density, kg/m^3
τ	stress tensor, Pa

Subscripts

w	wall
ave	average
b	bulk
in	inlet
out	outlet
$surf$	surface average
$line$	line average
$heat$	be heated

temperature gradient of the circumferential wall and can obtain a higher average heat transfer coefficient. Wang also found wrapped wire disrupted the regularity of the wall temperature distribution. In 2018, Z. Hu et al. (Hu et al., 2018) studied the heat transfer difference between a 2 × 2 bare rod bundle and a 2 × 2 wire-wrapped rod bundle experimentally. It is found that the heat transfer coefficient of the wire-wrapped rod bundle was 8.4% higher than that of the bare rod bundle. The existence of the wire can enhance heat transfer, but the flow parameters cannot be experimentally measured and the reasons for the heat transfer enhancement cannot be analyzed in detail.

To explain the influence of wrapped wire on heat transfer, many numerical simulation studies were carried out. In 2014, K. Podila and Y. Rao (Podila and Rao, 2014) studied the heat transfer of the supercritical water in the wire-wrapped rod bundle with the help of Computational Fluid Dynamics (CFD), since the calculation grid is highly inclined close to the wire, the treatment of approximating the wire to a semicircle was used to ensure high grid quality. In 2016, K. Podila and Y. Rao (Podila and Rao, 2016) also used a semicircular approximation to improve the mesh quality when studying convective heat transfer in 2 × 2 wire-wrapped rod bundles. This semicircular approximation is referenced from the method used by R. Wigeland and K. Hamman (Wigeland and Hamman, 2009) in their study of the electricity generation efficiency in the hexagonal fuel assembly of the sodium-cooled fast reactor. In fact, in 2010, K.D. Hamman and R.A. Berry (Hamman and Berry, 2010) put forward the idea that the physical model of wire loss embedding approximation cannot accurately simulate the actual situation and has the uncertainty of numerical models. Therefore, Hamman and Berry used a model with less wire loss to calculate the distribution of the sodium flow. Attila A. Kiss et al. (Kiss and Mervay, 2019; Kiss et al., 2015) embedded the wrapped wire in the rod bundle during analyzing the thermal-hydraulic effect of wrapped wire spacer in a four-rod fuel bundle and connected the wire to the rod bundle through sharp corners. When L. Liu et al. (Liu et al., 2017) studied the influence of the wire shape in the hexagonal fuel assembly rod bundle on the flow and heat transfer characteristics, the wires are embedded into the rod bundle by 0.1 mm to reduce the complexity of the geometric model.

There are also many studies on the effects of the wrapped wire in lead-bismuth and sodium-cooled fast reactors (Chen et al., 2018; He et al., 2021; Qin et al., 2019). D. Wang et al. (Wang et al., 2020) embedded the wire into the rod bundle 0.1 mm to reduce the difficulty of creating mesh while analyzing the thermal-hydraulic of a 7-pin sodium-cooled fast reactor wire- wrapped fuel bundle. J. Li et al. (Li et al., 2020) numerically study the 19-pin wire-wrapped assembly cooled by a lead-bismuth eutectic with the wire embedded into the rod bundle by 0.1 mm. Meanwhile, the wire structure is also recommended for small modular reactor (Bhowmik et al., 2021).

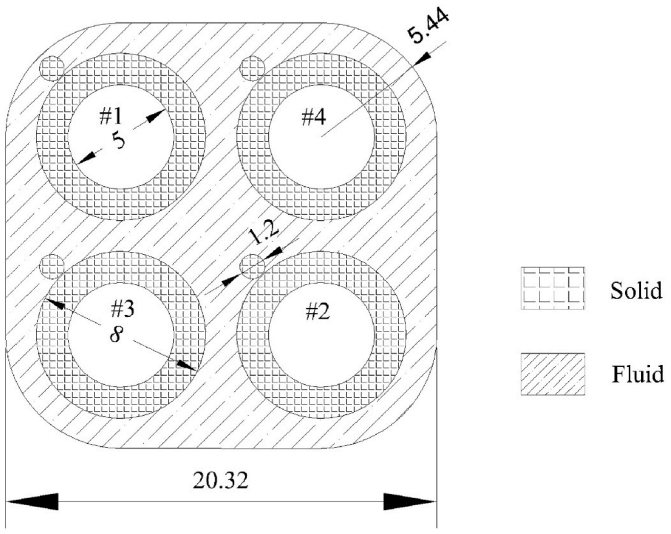

Fig. 1. Schematic diagram of the geometry of 2 × 2 wire-wrapped rod bundle.

From the above literature, it can be seen that most of the current studies of wire structures are simplified by the embedding approximation wire model, but this method has not been quantitatively evaluated. Also, the microscopic behavior of the fluid at the wire corners is currently under-studied due to the deficiencies of the model. Due to the wrapped wire loss model having uncertainty and cannot simulate the actual result accurately, a new type of high-fidelity non-destructive wrapped wire model is proposed. The model is generated by a hexahedral structured mesh and the wires are not embedded into the rod bundle, so the model can be simulated numerically with a very small grid number to obtain very accurate computational results. With the help of this model, this paper numerically studied the influence of the distance of wire embedded into the rod bundle d on the heat transfer and pressure drop and the microscopic behavior of the flow characteristics at the wire-rod corner of the wire. This numerical investigation can help to optimize the wire structure design while providing insight into the influence of wire. The structure of this paper is as follows: first, establish the high-fidelity non-destructive wrapped wire model and perform mesh sensitivity analysis. Then analyze the influence of the distance of wire

Table 1
Dimensions of 2 × 2 wire-wrapped rod bundle.

Geometry	Value
Outer diameter of heated rod	8.0 mm
Center distance between two rods	9.44 mm
Wall thickness of heated rod	1.5 mm
Diameter of wrapped wire	1.2 mm
Rod to wall-corner gap	1.44 mm
Flow area	181.91 mm^2
Effected heated length	600 mm
Pitch to diameter ratio	1.18
Pitch of wrapped wire	200 mm

Table 2
Physical conditions of 2 × 2 wire-wrapped rod bundle.

Parameter	Value
p (MPa)	25
W (g/s)	186.43 (Corresponding to the smooth rod bundle $G = 1000$ kg/ (m^2 ·s))
P (kW)	24.127 (Corresponding to the smooth rod bundle $q = 400$ kW/m^2)
T_{in} (K)	692.45

embedded into the rod bundle d on the heat transfer and pressure drop. Finally, the microscopic behavior of the flow characteristics at the wire-rod corner of the wire is explored.

2. Numerical approach

2.1. Physical model

The geometry structure is a 2 × 2 wire-wrapped rod bundle structure. The cross-sectional structure at the inlet is shown in Fig. 1. To describe the distribution of heat transfer characteristics of different rod bundles accurately, this paper defines 4 rod bundles as #1, #2, #3 and # 4 as shown in Fig. 1. The direction of rotation is counterclockwise. The geometric model fully conforms to the experimental structure of Wang's experiment (Wang et al., 2016). Detailed dimensions of the rod bundle and calculated geometric parameters of the wire-wrapped structure are listed in Table 1.

Wang's experimental data (Wang et al., 2016) are utilized to validate the accuracy of the non-destructive wire model. The specific physical boundary conditions are shown in Table 2. Boundary condition settings cover mass flow inlet, pressure outlet and constant body heat source power heating. To compare the difference in thermal-hydraulic characteristics of different geometric structures at the same total heating power and mass flow rate, the mass flux and body heat source power are determined by the following formula:

$$G = \frac{W}{A_{flow}} \tag{1}$$

$$q_v = \frac{P}{V_{heat}} \tag{2}$$

Where A_{flow} is the flow channel area and V_{heat} is the total heating volume, which are given by SolidWorks.

2.2. Meshing

A new structured meshing method based on a virtual ellipse flow surface and fillet connection was used to mesh 2 × 2 wire-wrapped rod bundle. In the existing studies on numerical simulations of wire-wrapped rod bundles, in general, the processing methods are to approximate the wrapped wire as a semicircle or embed the wire into the rod bundle for geometric simplification and meshing. These simplifications greatly reduce the difficulty of meshing, but at the same time reduce the size of the wire and thus the wire's ability to enhance turbulence. To accurately simulate the actual heat transfer, this paper uses ICEM to design a new type of high-fidelity non-destructive wrapped wire model that can make a lossless connection between the rod bundle and wire, thus ensuring that the physical model is completely consistent with the experiment.

This study sets up four virtual ellipse flow surfaces to divide the fluid domain into two parts, the inner and outer fluid domains. When dividing the outer fluid domain, the fluid domain is divided into 29 3D blocks. After vertex association, edge association and face association, the volume grids are generated which fits well with the virtual ellipse flow surface, as is shown in Fig. 2. In the inner fluid and solid domain, the volume grids are generated by 2D surface mesh rotation. The specific division of the 2D blocks is shown in Fig. 3. As shown in Fig. 3, the inner fluid domain and solid domain were divided into 21 and 15 2D blocks, respectively. Fig. 4 shows the cross-section meshing structure. To make the wire and the rod bundle approximately tangentially connected, this study uses a small fillet with a radius of 0.02 mm as shown in Fig. 4 to connect the wrapped wire and the rod bundle. Then the distance between the small round corners at both ends is only 0.4 mm, which can be approximately the length of the welding material required for spot welding. The ellipse flow surfaces greatly reduce the influence of the wire rotation on the fluid domain mesh and ensure the quality of the fluid domain mesh at a higher level. This meshing method makes it possible to evaluate the impact of wire-wound embedded rod bundles on numerical results. This paper compares and analyzes the non-destructive wrapped wire model with several models with different d. Fig. 5 is the schematic diagrams of the mesh which show the wrapped wire with different d.

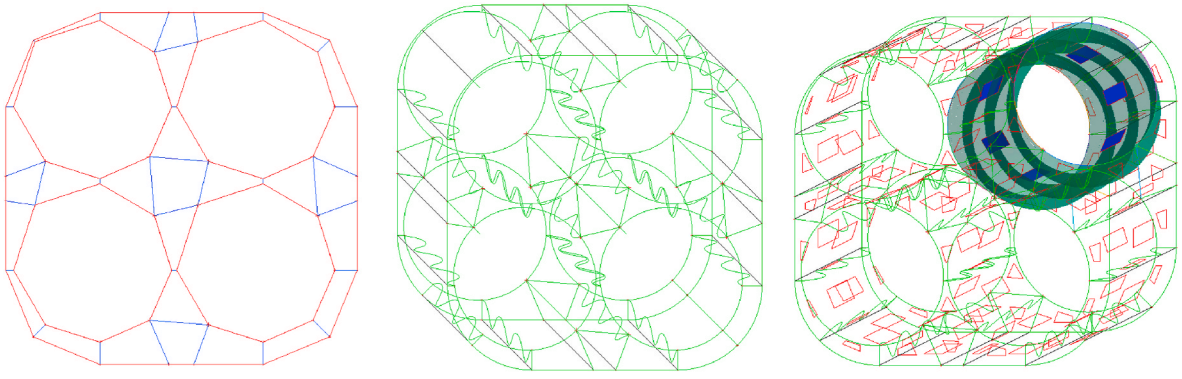

Fig. 2. Mesh methods of the outer fluid domain.

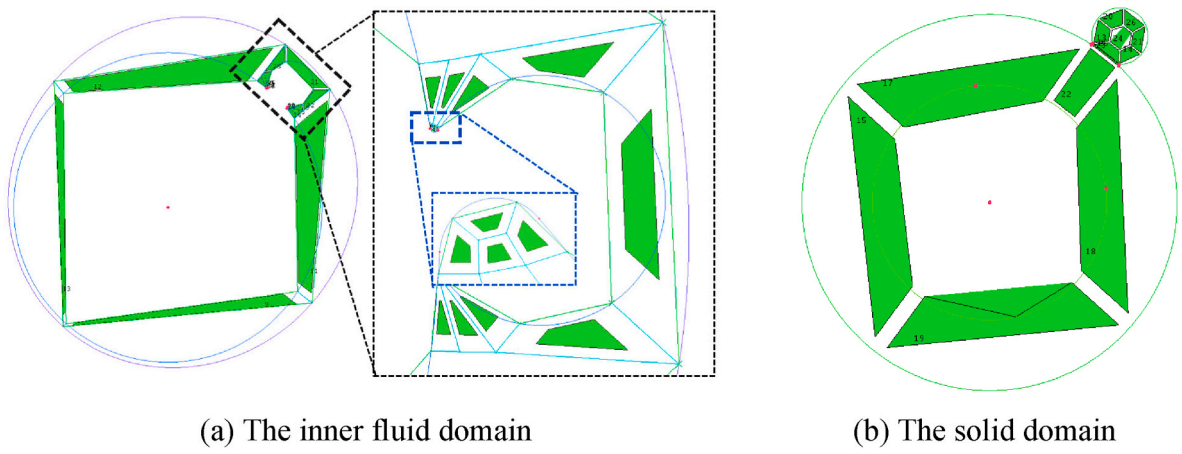

Fig. 3. Mesh methods of the inner fluid and solid domains.

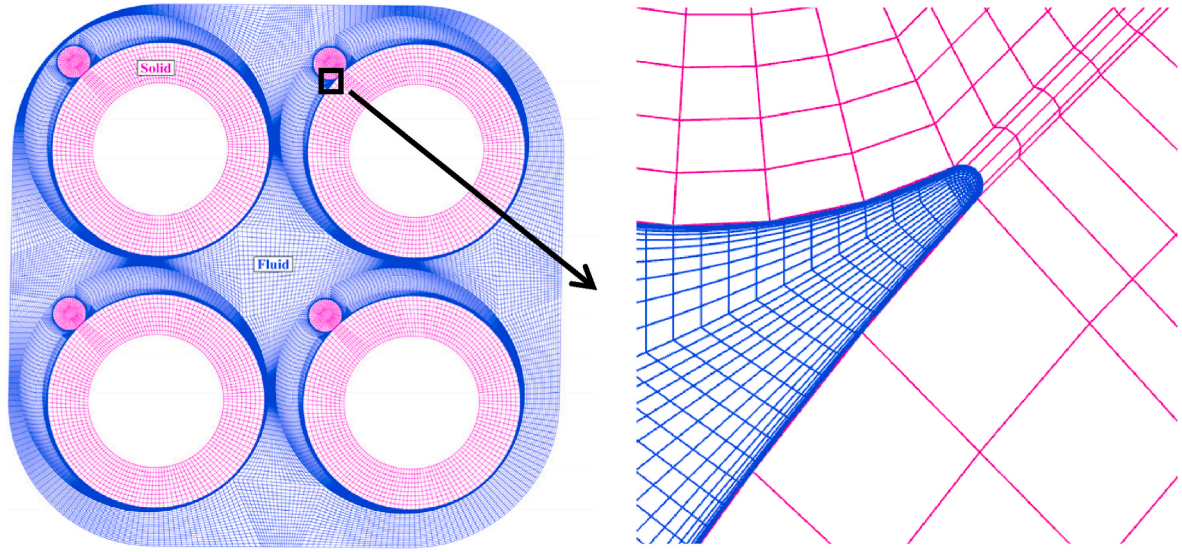

Fig. 4. Mesh partition on the cross-section and wire-rod contact corner.

2.3. Governing equations

The Governing equations are described as follows (Fluent, 2011).

Continuity:

$$\nabla \cdot (\rho|\vec{v}) = 0 \tag{3}$$

Momentum:

$$\nabla \cdot (\rho|\vec{v}|\vec{v}) = -\nabla p + \nabla \cdot (\bar{\bar{\tau}}) + \rho\vec{g} \tag{4}$$

Energy:

$$\nabla \cdot (\vec{v}|(\rho|E| + |p)) = \nabla \cdot \left(k_{eff}|\nabla|T| - |\sum_j h_j \vec{J_j}| + |(\bar{\bar{\tau}}_{eff}| \cdot |\vec{v}) \right) \tag{5}$$

Where p is the static pressure, $\bar{\bar{\tau}}$ is the stress tensor, k_{eff} is the effective conductivity ($k + k_t$, where k_t is the turbulent thermal conductivity, defined according to the turbulence model being used, $\vec{J}_j$ is the diffusion flux of species j. The first three terms on the right-hand side of Eq. (5) represent energy transfer due to conduction, species diffusion, and viscous dissipation, respectively.

2.4. Numerical simulation conditions

2.4.1. Mesh independence verification

In this paper, grid independence verification is performed based on the non-destructive wrapped wire model with the SST k-ω turbulence model. The boundary conditions are the same as Table 2. Due to the excessive node parameters of the structured mesh, we increase the number of nodes on every edge in equal proportion for mesh independence verification. Table 3 shows the calculated results of the pressure drop for different grid numbers. Fig. 6 shows the linear average wall temperature distribution of the rod bundle and the temperature and velocity distribution at the central axis along the axial direction. The linear average temperature of the rod bundle gradually increases with the increase of the grid number and then tends to be stable. When the number of grids exceeds 16.11 million, the maximum temperature difference of the local line average wall temperature doesn't exceed 0.2 K, the temperature and velocity distribution at the central axis no longer change and the pressure drop difference doesn't exceed 100 Pa at most. Therefore, it is considered that grid independence is achieved when the number of grids reaches 16.11 million. Considering the computation time and cost, ##3 is adopted in this paper, and the grid number of other models is similar to ##3.

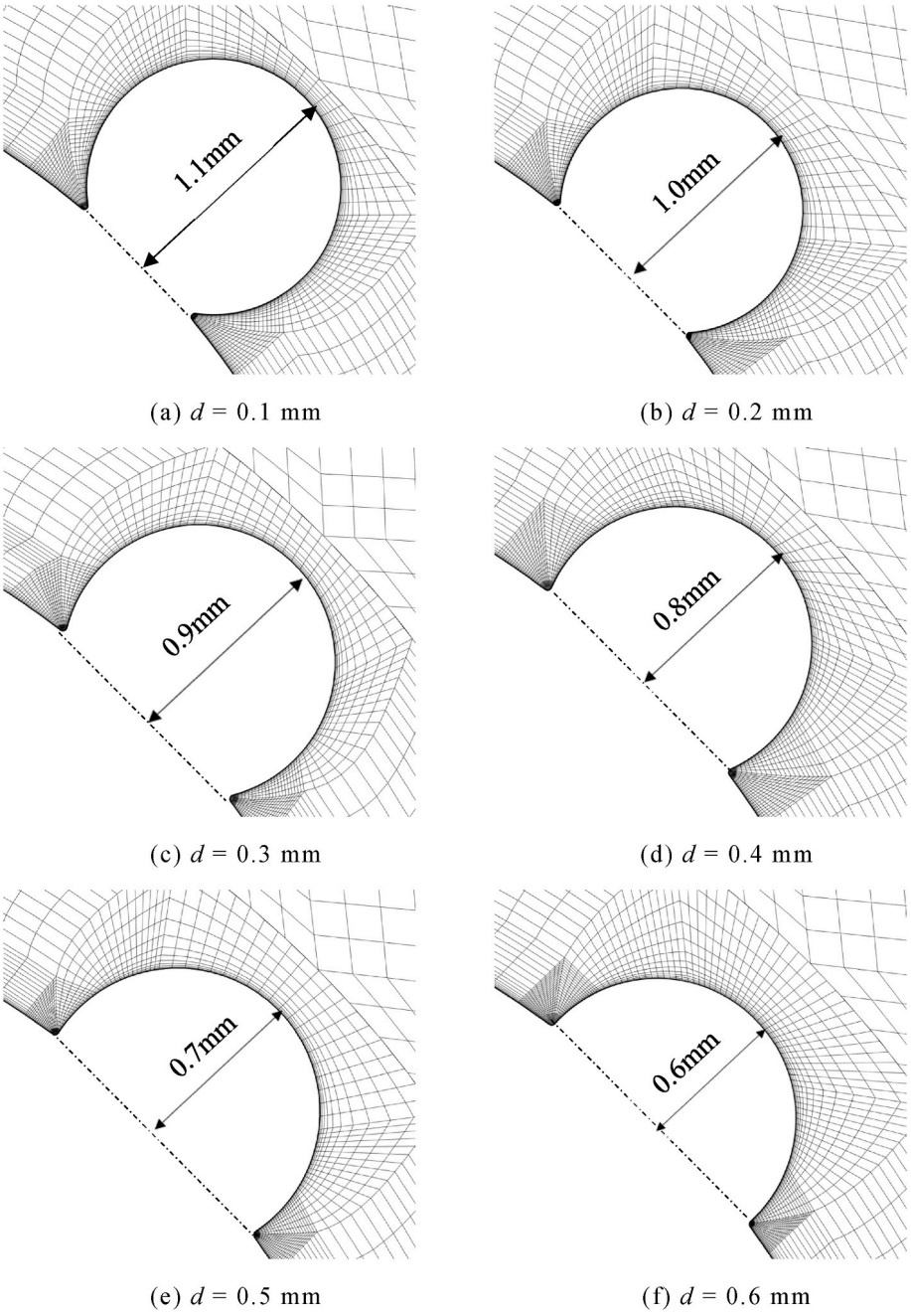

Fig. 5. Mesh partition of the wrapped wire with different *d*.

Table 3
Calculated results of the pressure drop for different grid numbers.

	##1	##2	##3	##4
number of mesh cells (million)	12.29	14.83	16.11	21.45
pressure drop (Pa)	13387.2	13081.1	13117.9	13175.3

2.4.2. Model validation

To satisfy $y^+ < 1$, the initial height of the first grid layer in this paper is 0.0005 mm. The computational results of SST *k-ω*, *ω*-RSM, BSL-RSM and Realizable *k-ε* models are selected for comparison with Wang's experimental data (Wang et al., 2016). Fig. 7 shows the comparison of the computational results of different turbulence models with the experimental data. The measurement uncertainty of the heat transfer coefficient in experiments is 8.83%.

The supercritical water is in the high enthalpy area in the calculation conditions. The enthalpy value is greater than 2700 kJ/kg. From Fig. 7, the calculation result of the ω-RSM turbulence model in the range is closer to the experimental data compared to other turbulence models. Therefore, *ω*-RSM turbulence model is selected. It needs to be emphasized that this high-fidelity wire-wrapped rod model proposed in this paper has a more accurate geometry compared to other models and is able to simulate the real experimental structure. Meanwhile, we compare the experimental data of the wall temperatures for different boundary conditions with the simulation results, as shown in Fig. 8. It can be seen that in the high enthalpy region, the turbulence model predictions are closer to the experimental values, which further validates the computational model.

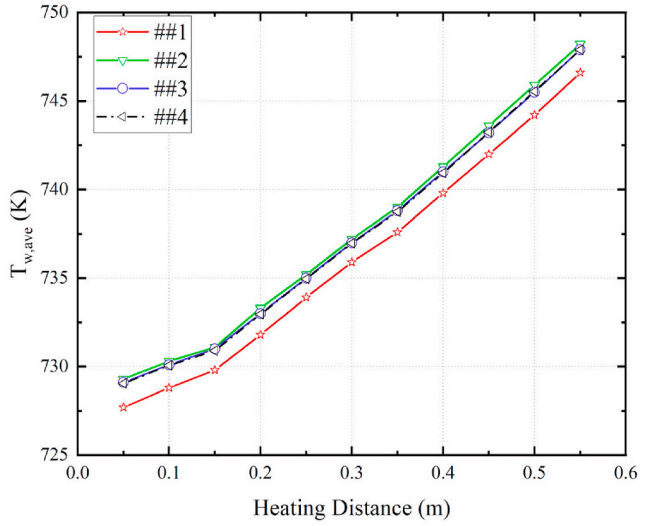

(a) The linear average wall temperature distribution of the rod bundle

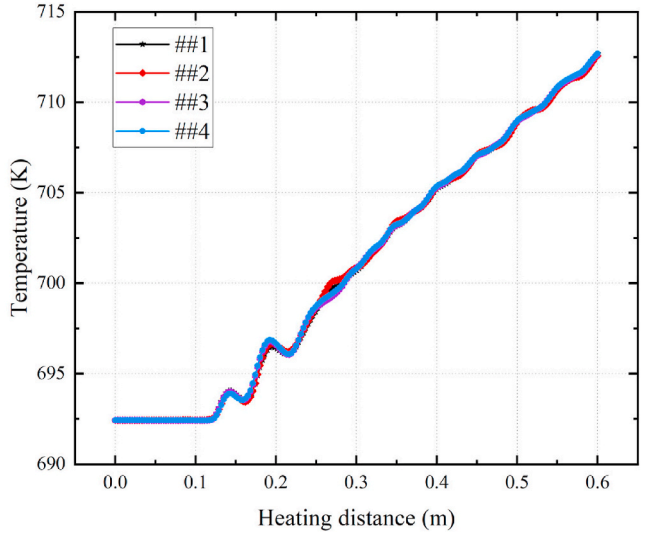

(b) The temperature distribution at the central axis

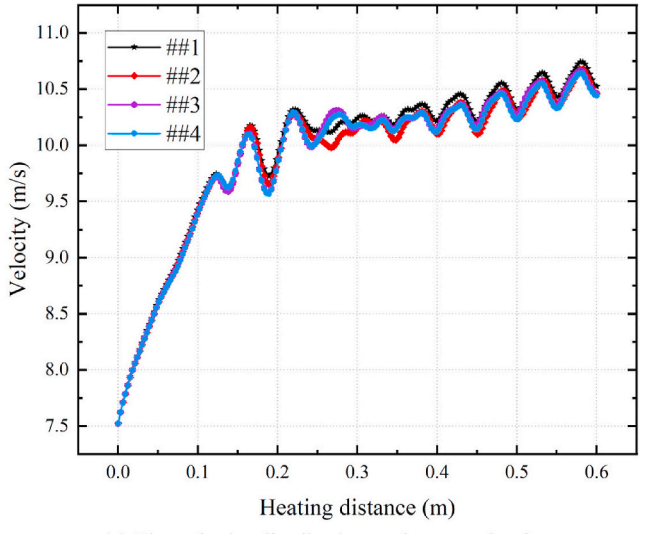

(c) The velocity distribution at the central axis

Fig. 6. Comparisons of numerical results with different grid numbers.

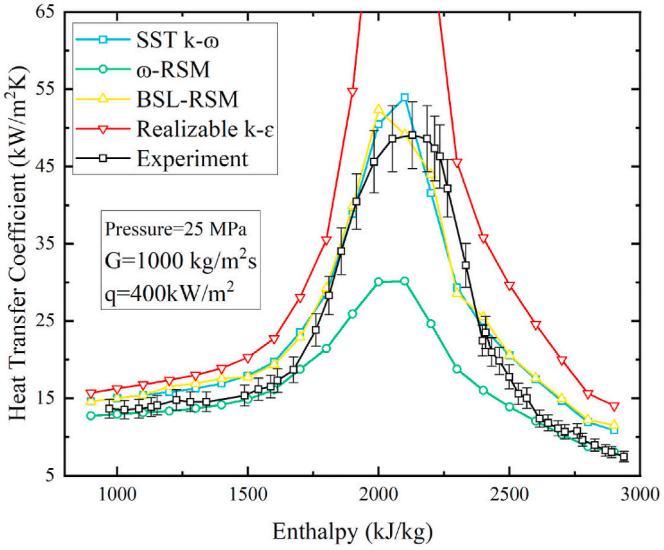

Fig. 7. Comparison between the calculation results of different turbulence models and the experimental data.

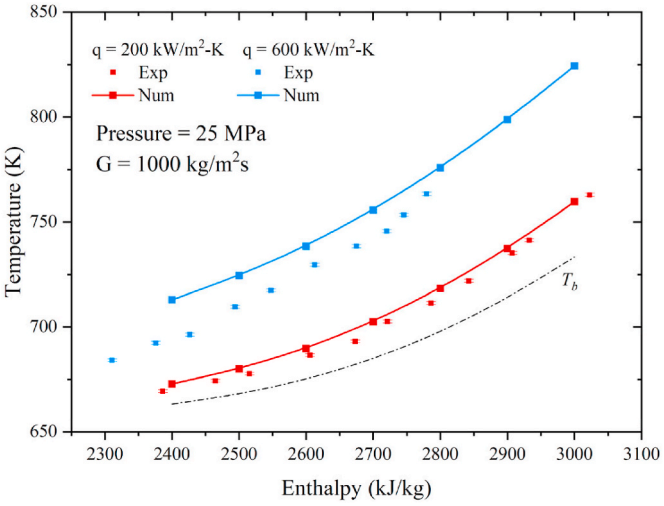

Fig. 8. Validation of ω-RSM turbulence model.

Table 4
Thermal physical properties of SS304.

Material	ρ (kg/m^3)	c_p (J/kg·K)	k (W/m·K)			
			20 °C	100 °C	300 °C	500 °C
SS304	7850	500	15	18	21	26

2.4.3. Numerical calculation conditions

The calculation software used in this paper is the commercial CFD software ANSYS FLUENT 2021R1, which uses the finite volume method to discretize the control equations and boundary conditions. In the solving process, the simple method and second-order upwind were applied to ensure an accurate simulation. The residual target was 1×10^{-4} for mass, stress, momentum and turbulent equations, and was 1×10^{-6} for energy. The simulation was converged after about 3000 iterations. The thermophysical properties of supercritical water were obtained from the NIST database (Lemmon et al., 2002) which has been implanted in FLUENT, and the solid material of the rod bundle is 304 stainless steel. The thermal conductivity of SS304 was fitting by

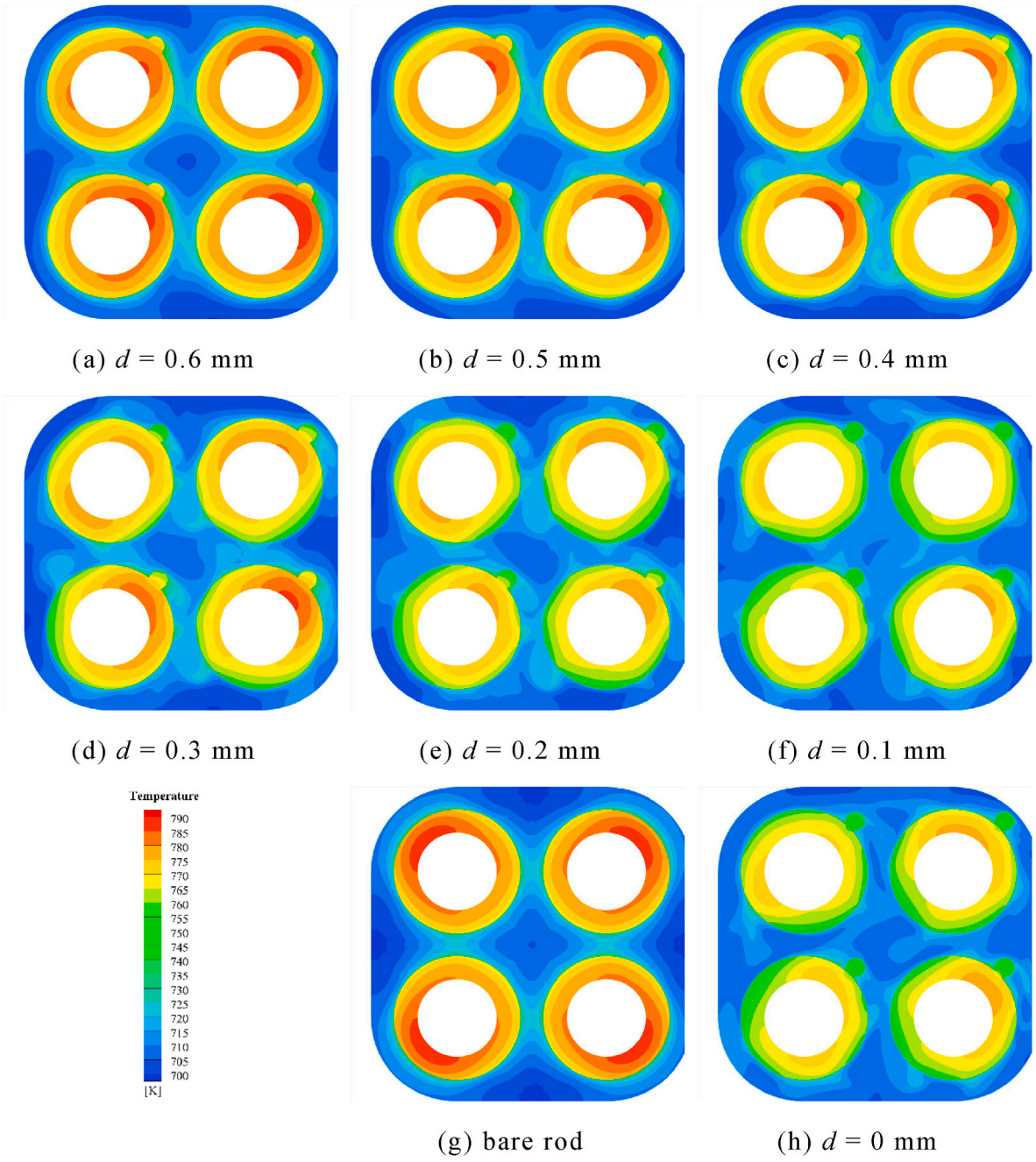

Fig. 9. Temperature contours at 550 mm from the inlet with different *d*.

piecewise linear. Specific physical properties parameters are shown in Table 4.

3. Result and discussion

3.1. Effects of wrapped wire loss on heat transfer

While analyzing the calculation results, the cross-section with the axial distance $z = 550$ mm from the inlet was selected as the study object. The simplified models with *d* of 0.1 mm, 0.2 mm, 0.3 mm, 0.4 mm, 0.5 mm, and 0.6 mm were compared to the bare rod bundle ($d = 1.2$ mm) and the non-destructive model for analysis. The temperature contours at 550 mm from the inlet are shown in Fig. 9. Compared with the calculated results of the non-destructive wire-wrapping model and the bare rod bundle model, the wire wrapping leads to a more uniform temperature distribution, which in turn enhances heat transfer. For different values of *d*, the loss of wire wrapping leads to a weakening in heat transfer. When $d = 0.6$ mm, the average wall temperature and the maximum temperature of the rod bundle are close to those of the bare rod bundle, while the position of the highest wall temperature is toward the direction of wire wrapping. The wall temperature distribution has obvious directionality, and the fluid temperature shows a similar distribution trend to that of the bare rod bundle. The temperatures in the inner and lateral subchannels are lower than in the other regions. When *d* is decreased to 0.3 mm, the direction of the highest wall temperature is still toward the direction of wire wrapping. However, the highest wall temperature and average wall temperature decrease, the heat transfer is enhanced, and the fluid temperature is more uniform than that when $d = 0.6$ mm. For *d* is reduced to 0.1 mm and the non-destructive wrapped wire model, the average temperature is lower, the maximum

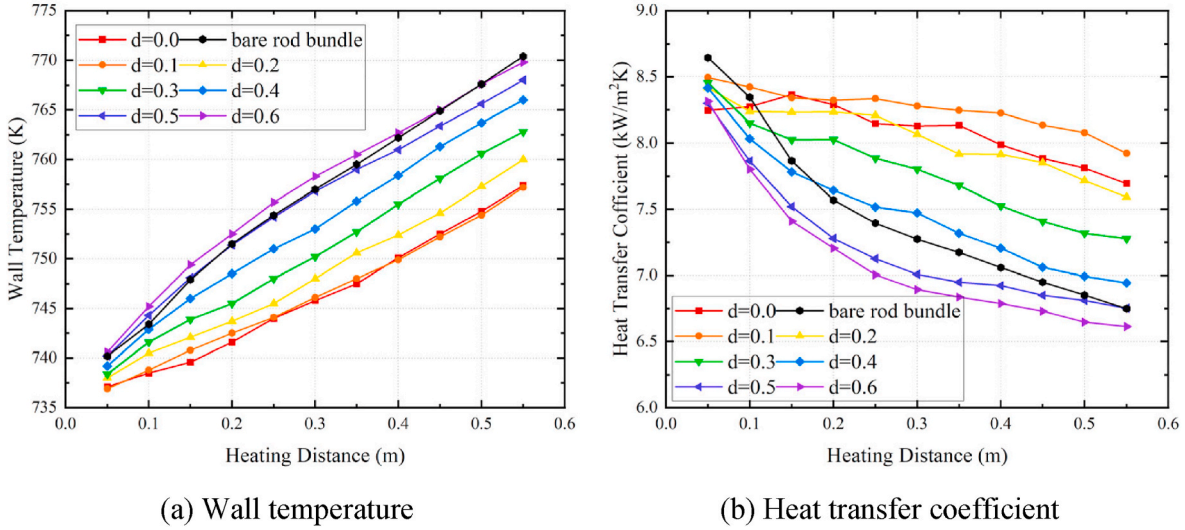

Fig. 10. The effects of d on wall temperature and heat transfer coefficient.

temperature distribution is not biased towards the wire direction, the heat transfer is further enhanced, and the fluid temperature distribution is more uniform. As the embedding distance d decreases, the average wall temperature and maximum wall temperature gradually decrease. The non-destructive wrap wire model exhibits the best heat transfer.

When the wire wrap model is oversimplified, e.g. $d = 0.6$ mm, the temperature calculation becomes inaccurate. #1 rod has a relatively high wall temperature near the wire. #2 has a higher maximum wall temperature than the other three rods, and #2 is the most susceptible to changes in d. The temperature distribution of #4 and #3 is similar to #2, but with a slightly lower wall temperature than #2. Low fluid temperatures are found in the internal subchannels and the lateral subchannels, which is similar to the case of the bare rod bundle.

In summary, the loss of the wire will weaken the heat transfer during the numerical calculation. The non-destructive wire-wrap model used in this study avoids this problem and brings the calculated results closer to the experimental situation. In this study, it is found that the calculation results of $d = 0.1$ mm do not differ much from those of the non-destructive wire-wrap model.

The linear average wall temperature and heat transfer coefficient at 11 positions along the axial direction with a step length of 0.05 m are shown in Fig. 10. The heat flux q and heat transfer coefficient h are defined as:

$$q = \frac{P}{A_{heat}} \tag{6}$$

$$h = \frac{q}{\overline{T_w} - T_b} \tag{7}$$

Where P is the total heating power, A_{heat} is the effective heating area. $\overline{T}_w$ is the wall temperature and T_b is the bulk-fluid temperature.

Fig. 10 shows the linear average temperature increases and the heat transfer coefficient decreases as the axial distance increases. When the wrapped wire loss is great, such as $d = 0.6$ mm and $d = 0.5$ mm, the variation trend of the linear average temperature and heat transfer coefficient is similar to that in the bare rod bundle model. Besides, the wall temperature is larger than that in the non-destructive wrapped wire model. As d decreases, the wall temperature gradually decreases and the decrease rate of heat transfer coefficient gradually slows down. When $d = 0.1$ mm or in the non-destructive wrapped wire model, the wall temperature shows similar and reaches the minimum, the decrease rate of the heat transfer coefficient is also low. In summary, the heat transfer

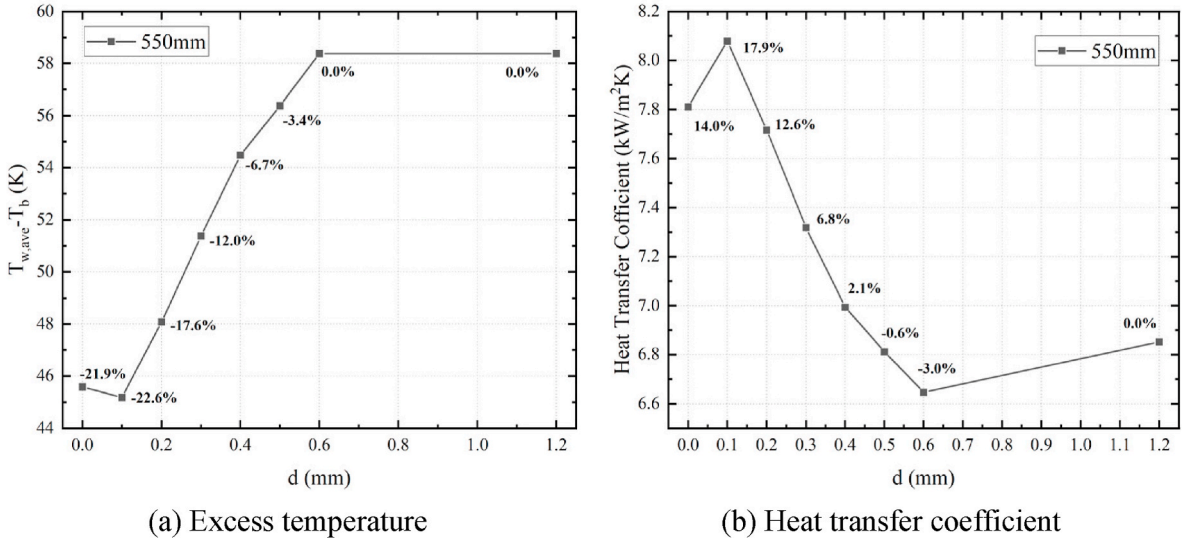

Fig. 11. Variation of wall temperature and heat transfer coefficient with d.

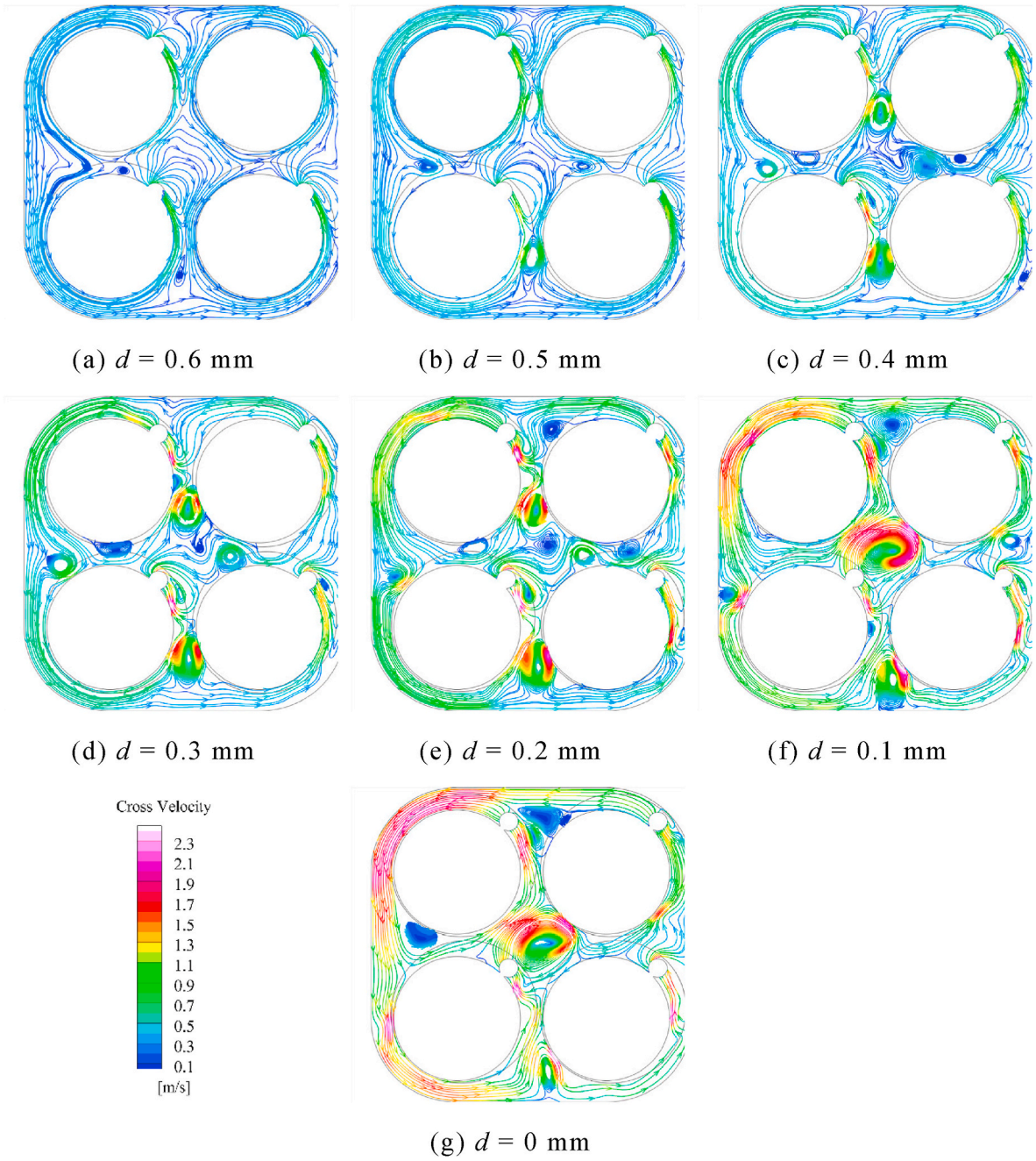

Fig. 12. Cross-sectional velocity and trace distribution with different *d*.

becomes better when *d* is small enough.

The numerical simulation results of the bare rod bundle are used as the benchmark to measure the heat transfer of models with different *d*. Fig. 11 shows the variation of wall temperature and heat transfer coefficient with *d*. As is shown in Fig. 9, when wrapped wire loss is excessive, such as $d = 0.6$ mm, the excess temperature is almost the same as the calculation result of the bare rod bundle, which is 58.38 K. As the embedding distance *d* decreases, the calculation results of wall temperature and heat transfer coefficient show almost linear changes compared with the result of the bare rod bundle, the wall temperature gradually decreases, the heat transfer coefficient gradually increases, and the heat transfer is enhanced. For $d = 0.1$ mm model or the non-destructive wrapped wire model, the wire average excess temperature is reduced by more than 20% and the heat transfer coefficient is increased by more than 10% compared with the bare rod bundle model ($h = 7.81, 8.08, 6.85$ kW/m^2·K for $d = 0, 0.1, 1.2$ mm). Therefore, if the wire-wrapped model is oversimplified for facilitating meshing, it cannot accurately simulate the actual situation. When the wire is properly embedded in the rod bundle, e.g., within 0.1 mm, the calculation results are similar to those of the non-destructive wire wrap model, with a relative error of no more than 1%.

The increase in embedding distance *d* essentially reduces the size of the wire, which affects the ability of the wire to enhance the formation of turbulence. The high-precision non-destructive wire wrap model proposed in this paper can solve this problem. To evaluate the effect of wrap-wire loss on turbulence formation, this paper applied the cross-sectional velocity v_{cross} to analyze the magnitude of lateral flow of fluid under the action of wrap-wire and explored the reasons for temperature variation. The distribution of the cross-sectional velocity v_{cross} is shown in Fig. 12, and the cross-sectional velocity v_{cross} is defined as

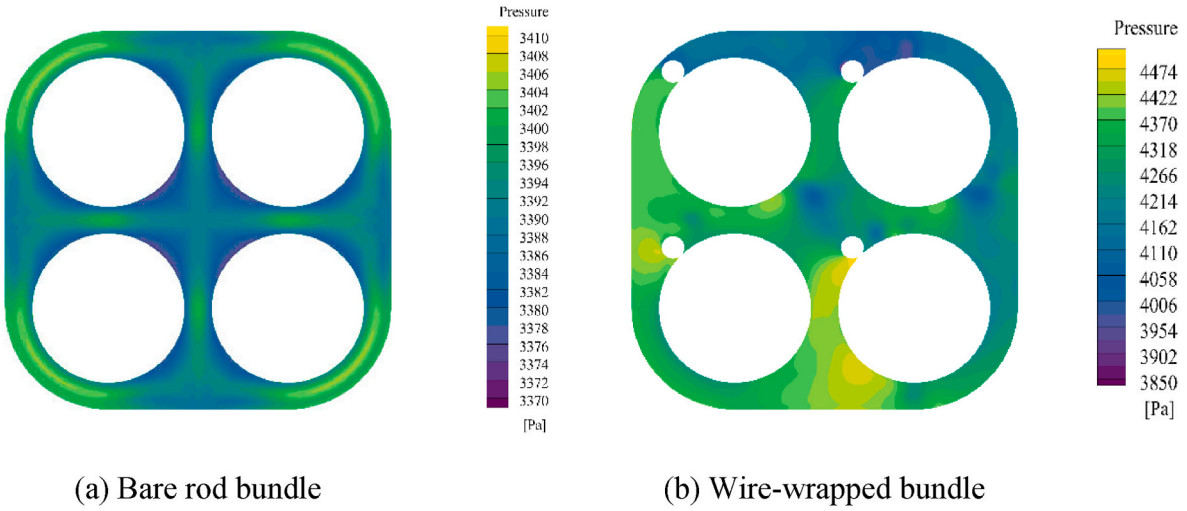

Fig. 13. Pressure distribution with or without wire.

follows:

$$v_{cross} = \sqrt{v_x^2 + v_y^2} \tag{8}$$

Where v_x is the velocity of the fluid along the x-axis and v_y is the velocity of the fluid along the y-axis. As is shown in Fig. 10, the formation of lateral flow increases with d decreases. When $d = 0.6$ mm, the cross-sectional velocity in the center sub-channel is lower than 0.5 m/s, and the lateral flow intensity is low. When $d = 0.3$ mm, the cross-sectional velocity increases, while the cross-sectional velocity around #1 and #3 in the corner sub-channel area increases more, the strength of the lateral flow increases, and vortexes appear in the edge sub-channels. When $d = 0.1$ mm and $d = 0$ mm, the cross-sectional velocity of the fluid around #1 and #3 increases, and the cross-sectional velocity in the edge sub-channels of #2 and #4 increases. When $d \leq 0.1$ mm, the lateral flow intensity is higher, a strong vortex is formed in the central sub-channel area, and strong vortices appear in the edge sub-channels.

In summary, excessive wrapped wire loss will seriously affect the intensity of turbulence and even lead to the failure of vortex formation. As embedding distance d decreases, the effect of the wire mixing the fluid and strengthening the formation of turbulence gradually increases. From the corresponding relationship between the cross-sectional velocity v_{cross} and the temperature distribution, the reason for the heat transfer enhancement with the decrease of embedding distance is due to the increase of transverse flow capacity of the wire mixing fluid and the increase of the number and intensity of vortices.

3.2. Effects of wrapped wire loss on pressure drop

Wire also interferes with the flow direction of the fluid and affects the local velocity, causing changes in the pressure distribution. Fig. 13 shows the contours of the pressure distribution section at $z = 400$ mm for the bare rod and non-destructive wire-wrapped models. The pressure distribution of the bare rod bundle in Fig. 11 is more uniform, and the pressure difference in the cross-section does not exceed 40 Pa. In the non-destructive wire-wrapped model, the pressure distribution is more chaotic, and the pressure difference in the cross-section is close to 700 Pa.

This paper applies the friction factor f as a parameter to characterize the pressure drop change, which is defined as:

$$f = \frac{2\Delta p_f D_{eq}}{LGv} \tag{9}$$

$$\Delta p_f = \Delta p - \rho_{ave} g(z_2| - |z_1) - G^2\left(v_{2,ave}| - |v_{1,ave}\right) \tag{10}$$

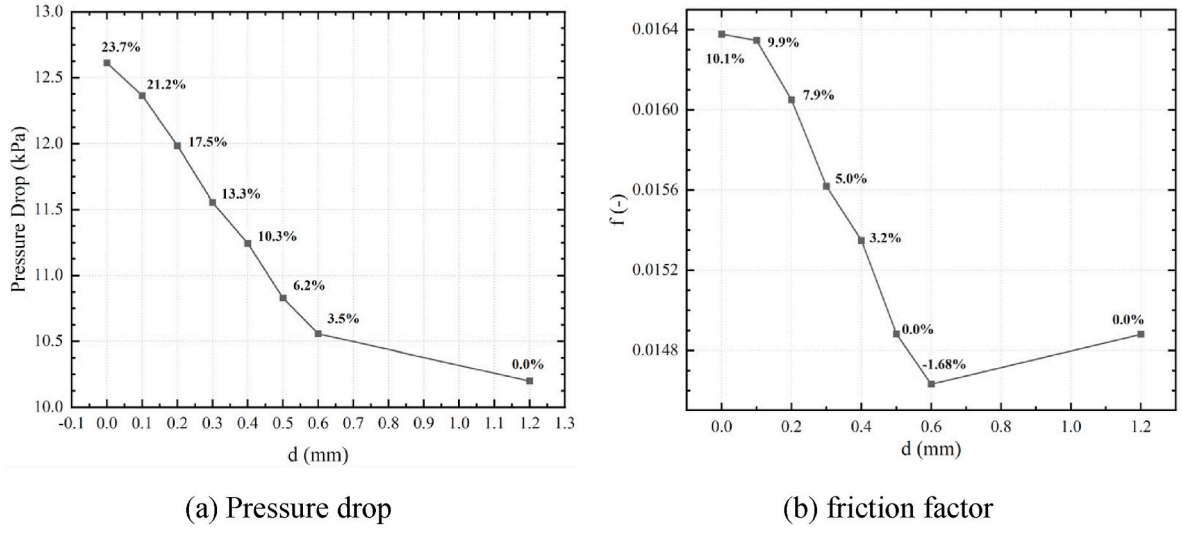

Fig. 14. Variation of pressure drop and friction factor with d.

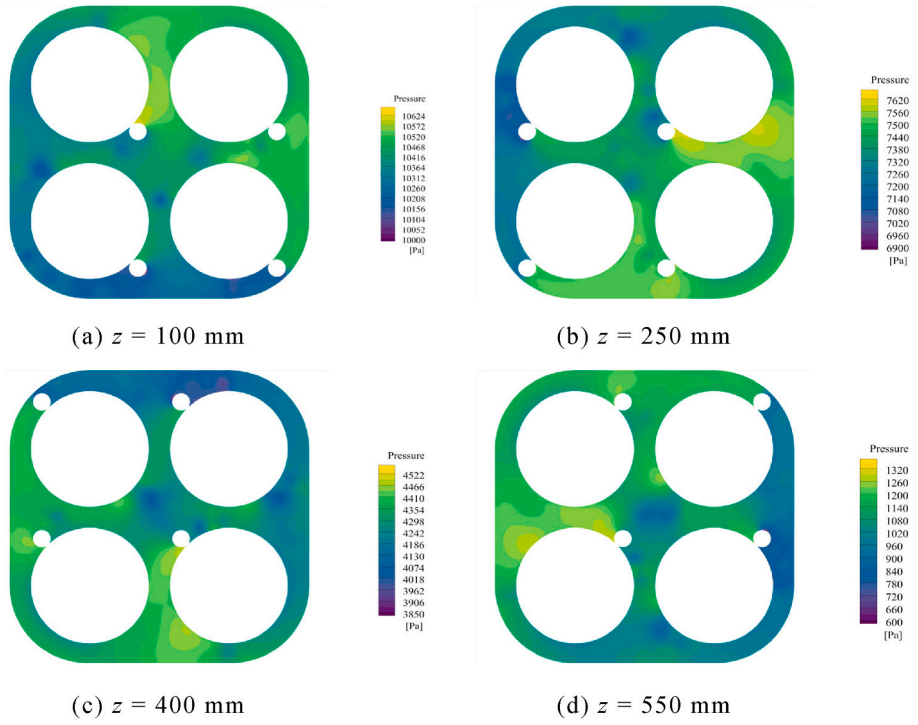

Fig. 15. Pressure contours at four cross-sections with the non-destructive wire model.

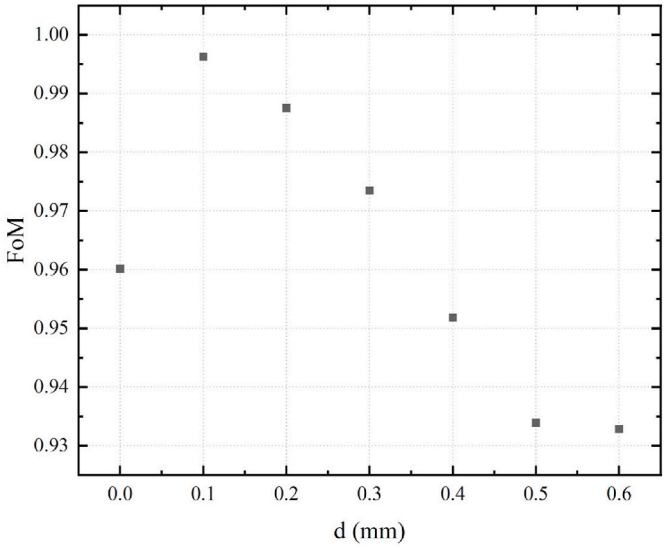

Fig. 16. FoM versus embedded distance *d*.

Where D_{eq} is the equivalent hydraulic diameter. Fig. 14 shows pressure drop and friction with different *d*, and the pressure of the bare rod bundle is used as a benchmark for comparison. As displayed in Fig. 14, the pressure drop increases with the decrease of *d*. When $d = 0.6$ mm, the pressure only increases by 3.5% compared with the bare rod bundle. The pressure and friction factor of $d = 0.1$ mm are similar to the non-destructive wrapped wire model, which increases by 23.7% and 10.1% respectively. When $d \geq 0.5$ mm, the friction factor is almost the same as that of the bare rod bundle. The influence of the wrapped wire loss on the pressure change exceeds 2 kPa, which is close to a gap of 20%. In terms of pressure changes, the calculation result of $d = 0.1$ mm is similar to the calculation results of the non-destructive wire-wrapped model. It can be considered that $d \leq 0.1$ mm is within the acceptable range for numerical simulation.

To explore the influence of wrapped wire on the pressure distribution, this paper takes the pressure contour at the axial distance of 100 mm, 250 mm, 400 mm and 550 mm respectively for comparison and analysis, as shown in Fig. 15. The locations with higher pressure are distributed in the counterclockwise direction of the wrapped wire, which is consistent with the direction of the wrapped wire, and the locations with lower pressure are concentrated in the side sub-channel and the corner channel. This distribution changes periodically.

3.3. Combined effect of wire on heat transfer and pressure drop

To evaluate the combined effect of wire on heat transfer enhancement and pressure drop increase, we refer to the work of M. H. Tusar et al. (Tusar et al., 2021) and use the evaluation factor FoM, defined in Eq. (11), and the corresponding FoM values with different *d* are shown in Fig. 16. It can be seen that the value of FoM increases firstly with the increase of the embedding distance *d*, and achieves a great value when $d = 0.1$ mm, and then decreases. This indicates that the combined effect of heat transfer and pressure drop increase is best at $d = 0.1$ mm. Also, it can be noted that the FoM value is always less than 1, which is caused by the greater influence of the wire on the hydraulic diameter. The values of the hydraulic diameter under different $d = 0$–0.6 mm are 3.94 mm, 4.00 mm, 4.05 mm, 4.09 mm, 4.12 mm, 4.16 mm and 4.19 mm, which are much smaller compared with the hydraulic diameter of 4.32 mm at the bare rod bundle.

$$FoM = \frac{(N|u|/|N|u_{bare})}{(f|/|f_{bare})^{\frac{1}{3}}} \tag{11}$$

3.4. Microscopic behavior at the wire-rod corner

The non-destructive wire wrap model can more accurately simulate the flow characteristics at the wire-rod contact corner. Fig. 17 shows the contours of temperature, density and velocity distributions of fluid microscopic behavior near the wire in the non-destructive wire wrap model for #3 at $z = 550$ mm.

As shown in Fig. 17, the microscopic behavior near the wrapped wire

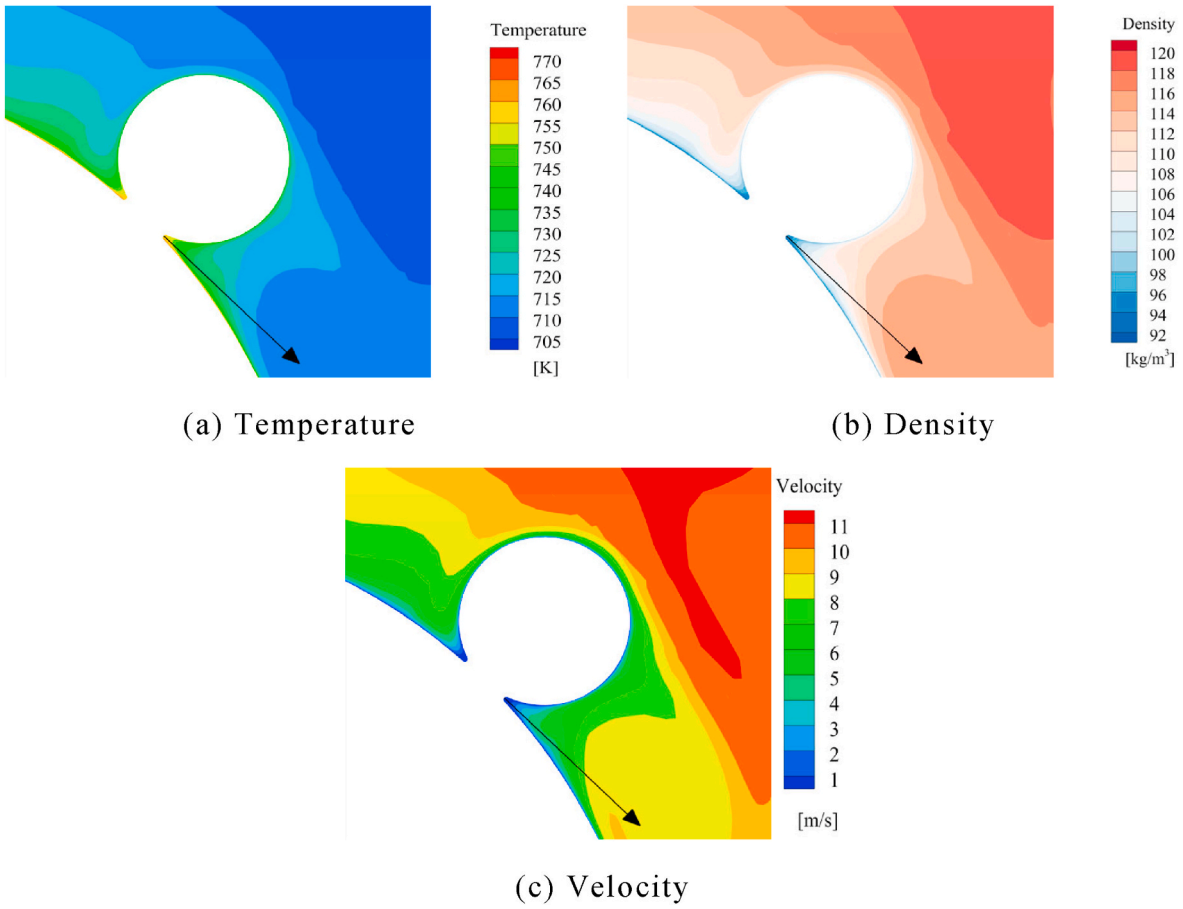

Fig. 17. Different contours of microscopic behavior near the wrapped wire.

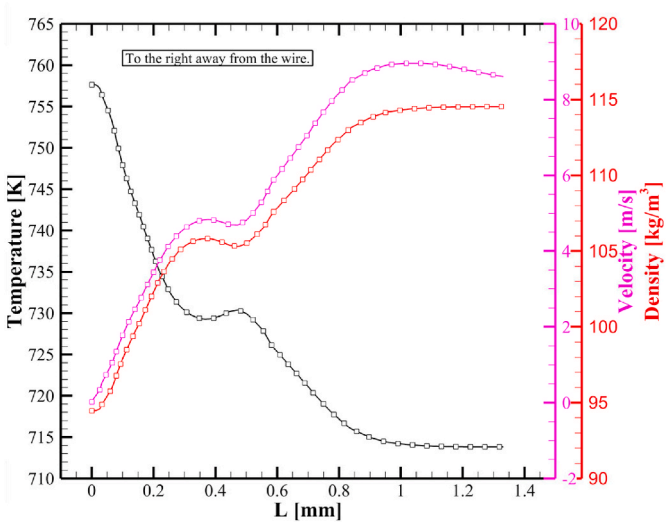

Fig. 18. Variation of temperature, velocity and density with distance from wire-rod contact corner.

shows slow velocity high temperature and low density. At the wire-rod contact corner, due to the boundary layer effect, the fluid at the corner forms a dead water area. In this area, the velocity of the fluid is relatively low, almost close to 0 m/s, which forms a large gap with the flow velocity of the mainstream area greater than 10 m/s. Due to the low flow velocity, the temperature of the fluid in this area is relatively high, 70 K higher than that of the fluid in the mainstream area, forming a large temperature gap. Because the radial temperature gap is too large, the density of the fluid also varies greatly, resulting in low fluid density in the dead water area and high density in the mainstream area.

Fig. 18 shows the temperature, velocity and density changes along the tangent direction at the wire-rod corner. When the distance from the inner wall is greater than 0.01 mm, the temperature, density and velocity show a sudden trend of accelerating, then slowly changing, and then sharply changing. As can be seen from Fig. 18, the dead water zone is formed within approximately 0.6 mm from the inner wall. The heat transfer and flow characteristics in this region change sharply and are prone to impurity deposition.

Fig. 19 shows the flow trace and the pressure, temperature, density, and velocity distributions of #3 and #1 from z = 530 mm–560 mm. Fig. 17 shows the detailed flow trace at the wire-rod contact corner of wire #3. From Fig. 19, the fluid flow and heat transfer characteristics and distribution trends are not much different at different rod bundle positions. At the same time, the fluid in the counterclockwise direction of the wire and the clockwise direction of the wire have the same flow trend. As is shown in Fig. 20, the fluid moves more than 30 mm at the wire-rod contact corner. This is another reason for the excessively high temperature in the dead water area at the wire-rod contact corner.

In summary, due to low flow velocity and long flow distance at the wire-rod contact corner, the fluid temperature is high and the density is low, forming an obvious dead water area.

4. Conclusion

This study is based on Wang Han's experiment at the working pressure of 25 MPa, inlet temperature of 692.45 K, mass flux of 1000 kg/m^2·s, and heat flux of 400 kW/m^2. A high-fidelity 2 × 2 wire-wrapped

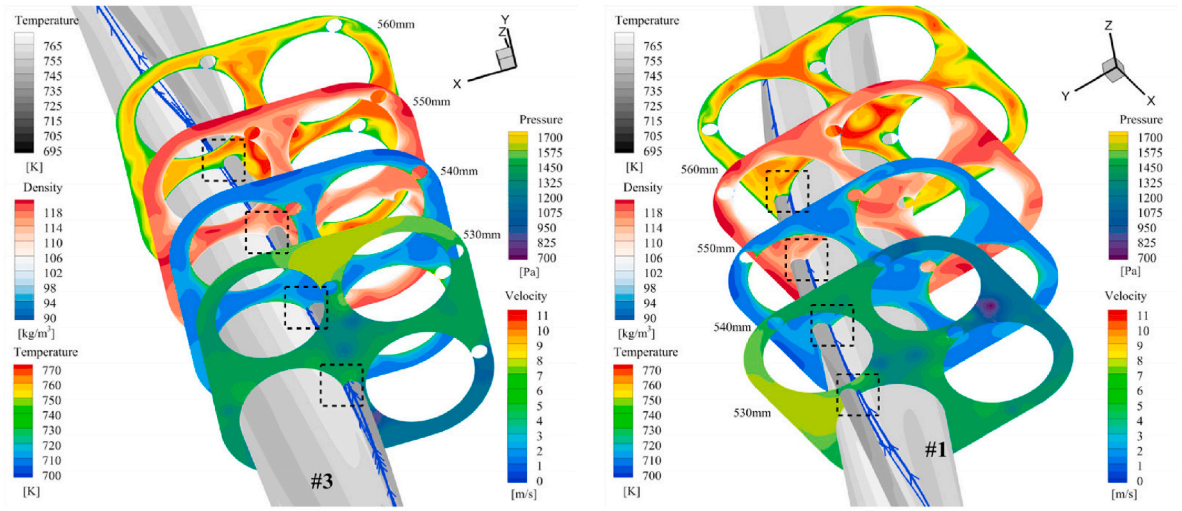

Fig. 19. Flow characteristics of #3 and #1.

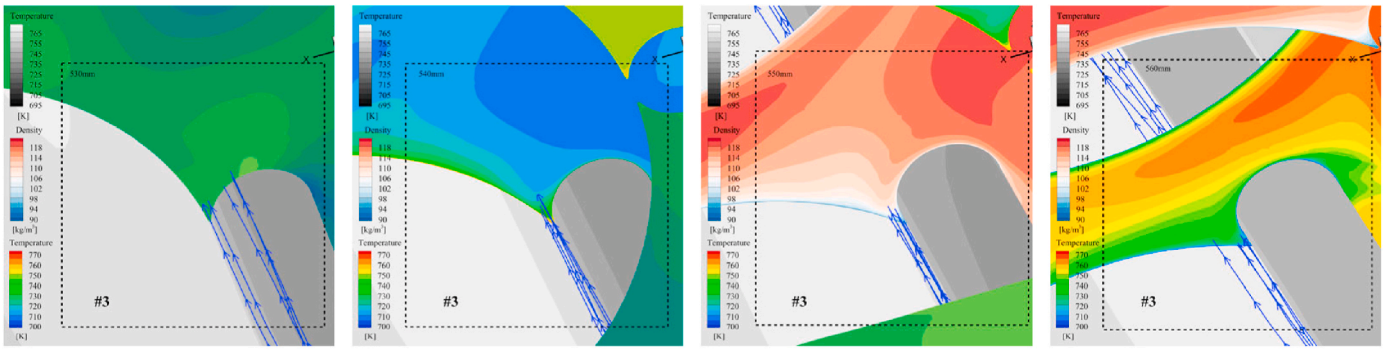

Fig. 20. Trace distribution at wire-rod contact corner of #3.

rod model designed by fillet connection and virtual ellipse flow surface is proposed for numerical simulation. Through the evaluation and comparison of the heat transfer and pressure drop changes in different wrapped wire loss models, the advantages of the non-destructive wrapped wire model on numerical simulation calculation are reflected. By high-fidelity non-destructive wrapped wire model based on virtual flow surface and fillet connection, the microscopic behavior at the wire-rod contact corner is analyzed in detail. Conclusions as below:

1. The heat transfer and flow characteristics of the non-destructive wrapped wire model are more consistent with the experiment. Non-destructive wrapped wire model shows higher accuracy than the wrapped wire loss model. By comparison, the difference in wall temperature when the distance of wire embedded into the rod bundle d is 0.1 mm is less than 1% compared with that of the non-destructive wrapped wire model. Therefore, this paper considers the acceptable range for the wire to be embedded into the rod bundle by 0.1 mm.

2. Wire can mix fluid and enhance heat transfer. As the embedding distance decreases, the degree of mixing is enhanced, thereby enhancing heat transfer. In this study, compared with the bare rod bundle, the wrapped wire reduce the wall temperature by more than 21.9% and the heat transfer coefficient increased by 14.0%.

3. The pressure drop variation has obvious periodicity and its trend is related to the direction of the wire. As the embedding distance is smaller, the pressure drop and the friction factor gradually increased. In this study, compared the calculation results with the bare rod bundle, the wrapped wire increases pressure drop by 23.7% and increases friction factor by 10.1%.

4. Due to low flow velocity and long flow distance at the wire-rod contact corner, the fluid temperature is high and the density is low, forming an obvious dead water area. The characteristics difference between dead water area and mainstream area are large. The gradient of change along the tangential direction of the wire-rod contact corner is large in the dead water area. In practical applications, it is easy to form impurity deposits in this area.

Declaration of competing interest

The authors declare that they have no known competing financial interests or personal relationships that could have appeared to influence the work reported in this paper.

Data availability

The data used has been cited.

References

Bhowmik, P.K., Shamim, J.A., Chen, X., Suh, K.Y., 2021. Rod bundle thermal-hydraulics experiment with water and water-Al2O3 nanofluid for small modular reactor. Ann. Nucl. Energy 150.

Chen, J., Zhang, D., Song, P., Wang, X., Wang, S., Liang, Y., Qiu, S., Zhang, Y., Wang, M., Su, G.H., 2018. CFD investigation on thermal-hydraulic behaviors of a wire-wrapped fuel subassembly for sodium-cooled fast reactor. Ann. Nucl. Energy 113, 256–269.

Cheng, X., Schulenberg, T., Bittermann, D., Rau, P., 2003. Design analysis of core assemblies for supercritical pressure conditions. Nucl. Eng. Des. 223, 279–294.

DoE, U., 2002. A technology roadmap for generation IV nuclear energy systems. http://gif.inel.gov/roadmap/pdfs/gen.iv.roadmap.pdf.

Fluent, A., 2011. Ansys Fluent Theory Guide, vol. 15317. Ansys Inc., USA, pp. 724–746.

Gu, H.-Y., Hu, Z.-X., Liu, D., Li, H.-B., Zhao, M., Cheng, X., 2016. Experimental study on heat transfer to supercritical water in 2× 2 rod bundle with wire wraps. Exp. Therm. Fluid Sci. 70, 17–28.

Gu, H., Li, H., Hu, Z., Liu, D., Zhao, M., 2015. Heat transfer to supercritical water in a 2× 2 rod bundle. Ann. Nucl. Energy 83, 114–124.

Hamman, K.D., Berry, R.A., 2010. A CFD simulation process for fast reactor fuel assemblies. Nucl. Eng. Des. 240, 2304–2312.

He, S., Wang, M., Zhang, J., Tian, W., Qiu, S., Su, G.H., 2021. Numerical simulation of three-dimensional flow and heat transfer characteristics of liquid lead–bismuth. Nucl. Eng. Technol. 53, 1834–1845.

Hofmeister, J., Waata, C., Starflinger, J., Schulenberg, T., Laurien, E., 2007. Fuel assembly design study for a reactor with supercritical water. Nucl. Eng. Des. 237, 1513–1521.

Hu, Z., Li, H., Tao, J., Liu, D., Gu, H., 2018. Experimental study on heat transfer of supercritical water flowing upward and downward in 2× 2 rod bundle with wrapped wire. Ann. Nucl. Energy 111, 50–58.

Kiss, A., Mervay, B., 2019. Numerical analysis on the thermal hydraulic effect of wrapped wire spacer in a four rod fuel bundle. Nucl. Eng. Des. 342, 276–307.

Kiss, A., Vágo, T., Aszódi, A., 2015. Numerical analysis on inlet and outlet sections of a test fuel assembly for a Supercritical Water Reactor. Nucl. Eng. Des. 295, 415–428.

Lemmon, E.W., Huber, M.L., McLinden, M.O., 2002. NIST reference fluid thermodynamic and transport properties–REFPROP. In: NIST Standard Reference Database, 23 v7.

Li, J., Fang, D., Guo, C., Wang, M., Deng, J., Tian, W., Qiu, S., Su, G.H., 2020. Numerical study on the thermal hydraulic characteristics in a wire-wrapped assembly of LFRs. Front. Energy Res. 8.

Liu, L., Wang, S., Bai, B., 2017. Thermal-hydraulic comparisons of 19-pin rod bundles with four circular and trapezoid shaped wire wraps. Nucl. Eng. Des. 318, 213–230.

Oka, Y., Koshizuka, S.-i., Ishiwatari, Y., Yamaji, A., 2002. Elements of Design Consideration of Once-Through Cycle, Supercritical-Pressure Light Water Cooled Reactor, vol. 555. American Nuclear Society, La Grange Park, IL. North Kensington Avenue,.

Podila, K., Rao, Y., 2014. Assessment of CFD for the Canadian SCWR bundle with wire wraps. Prog. Nucl. Energy 77, 373–380.

Podila, K., Rao, Y., 2016. CFD modelling of supercritical water flow and heat transfer in a 2× 2 fuel rod bundle. Nucl. Eng. Des. 301, 279–289.

Qin, H., Wang, C., Wang, M., Zhang, D., Tian, W., Su, G.H., Qiu, S., 2019. Numerical investigation on thermal-hydraulic characteristics of NaK in a helical wire wrapped annulus. Int. J. Heat Mass Tran. 145.

Squarer, D., Schulenberg, T., Struwe, D., Oka, Y., Bittermann, D., Aksan, N., Maraczy, C., Kyrki-Rajamäki, R., Souyri, A., Dumaz, P., 2003. High performance light water reactor. Nucl. Eng. Des. 221, 167–180.

Tusar, M.H., Bhowmik, P.K., Salam, B., Uddin Ahamed, J., Kim, J.K., 2021. Convective heat transfer and friction factor characteristics of helical strip inserted annuli at turbulent flow. Int. J. Heat Mass Tran. 176.

Wang, D., Peng, C., Guo, Y., 2020. Thermal-hydraulic analysis of a 7-pin sodium-cooled fast reactor wire-wrapped fuel bundle. Int. J. Heat Mass Tran. 160.

Wang, H., Bi, Q., Leung, L.K., 2016. Heat transfer from a 2× 2 wire-wrapped rod bundle to supercritical pressure water. Int. J. Heat Mass Tran. 97, 486–501.

Wang, H., Bi, Q., Wang, L., Lv, H., Leung, L.K., 2014. Experimental investigation of heat transfer from a 2× 2 rod bundle to supercritical pressure water. Nucl. Eng. Des. 275, 205–218.

Wigeland, R., Hamman, K., 2009. Fast Reactor Subassembly Design Modifications for Increasing Electricity Generation Efficiency. Idaho National Lab.(INL), Idaho Falls, ID (United States).

Yamaji, A., 2001. Conceptual core design of a 1000MWe supercritical-pressure light water cooled and moderated reactor. In: Proc. Am. Nucl. Soc. and Health Phys. Soc. Student Conf.. March 29-April 1, 2001, Texas, USA.

Zhao, M., Gu, H., Cheng, X., 2012. Experimental Study on Heat Transfer to Supercritical Water Flowing through Tubes, vol. 555. American Nuclear Society, La Grange Park, IL. North Kensington Avenue.